PROCEEDINGS, Thirty-Fifth Workshop on Geothermal Reservoir Engineering
Stanford University, Stanford, California, February 1-3, 2010
SGP-TR-188

HYDRAULIC FRACTURING OF NATURALLY FRACTURED RESERVOIRS

R.G. Jeffrey, X. Zhang, and A.P. Bunger

CSIRO Earth Science and Resource Engineering
Ian Wark Laboratory
Melbourne, Victoria, 3168, Australia,
Rob.Jeffrey@csiro.au

ABSTRACT

A carefully engineered stimulation that makes use of opening mode fractures is an effective way to reduce injection and production impedance and provide better access for the fluid to enter and promote shearing in the main reservoir volume. We present results from field experiments that mapped the fracture geometry for opening mode hydraulic fractures formed in naturally fractured crystalline rock masses. The propped fractures were formed by water and crosslinked gel fluids injected at relatively low rates (300 to 400 Liters per minute), but into a short isolated zone. The fractures formed were mapped after mining. The fractures consisted of one dominant propped channel that was offset at some shear and vein structures. Numerical modeling indicates that a stepped fracture path requires higher pressure to extend and extends more slowly than a straight fracture path. The shear displacement that is generated on the fracture path leads to self propping. We conclude that it is practical to place unpropped and propped opening mode fractures into naturally fractured rock to reduce flow impedance of the well and improved stimulation of EGS reservoirs.

INTRODUCTION

Stimulation of geothermal reservoirs, especially hot fractured rock or enhanced geothermal systems (EGS) reservoirs, has usually relied on injection of thin or low viscosity fluids (e.g. water) at pressures that are below the fracture opening pressure. The fluid is injected into a relatively long openhole section of the well with the intent that fluid will enter and pressurize a large zone extending from the well into the reservoir. As the pressure in the rock mass is increased, the effective normal stress acting across natural fractures in the rock is decreased, promoting shear slippage along some of these fractures. Thus, by the process of shear-induced dilation, the conductivity of the natural fractures is enhanced and a higher-permeability reservoir is formed (Pearson, 1981; Pine and Batchelor, 1984).

Conventional opening mode hydraulic fracturing has been applied to geothermal and EGS reservoirs in the past and has provided a stimulation effect. A recent example is described by Zimmerman et al. (2008) in stimulating a fractured volcanic sequence in a geothermal research well at Gross Schoenenbeck in Germany. However, the application of opening mode hydraulic fractures to EGS reservoirs is not widely accepted as a useful approach to stimulation.

In the following sections we will first briefly review opening and shear mode fracturing to provide a background for the data following. We will then describe the site conditions and fracturing treatments carried out as part of a trial to measure hydraulic fracture growth at a mine site. Results of the mine through and modeling of the fracture geometry mapped are then discussed.

HYDRAULIC FRACTURING

Hydraulic fracturing is widely used in the oil and gas industry to stimulate production from wells. In that application, the fractures are typically created under conditions with lower in situ stresses and with higher injection rates and pressures than in geothermal applications. Here the hydraulic fractures are predominantly opening mode, oriented such that the opening is aligned with the least compressive in situ stress. Typically a slurry of fluid and proppant, often sand, is pumped during the treatment so that after injection has ceased and the pressure has dissipated, a high permeability proppant-filled crack will remain. However, even in the absence of proppant, stimulation of permeability can be achieved due to the creation of new fractures, fracturing any minerals that are cementing a natural fracture closed, and/or through the residual opening that results from the fact that even opening mode fractures can be expected to be accompanied by some shear displacement, leading to a mismatch between the asperities on opposing fracture surfaces. This is especially true in naturally fractured rock, as will be discussed in more detail below, after the mined fractures are described.

In contrast, geothermal stimulation generally takes place under conditions with high in situ stresses and relatively low injection rates. Pressures are usually limited so they never exceed the minimum stress magnitude. Here the hydraulic fractures are expected to be predominantly shearing mode. The stimulation will therefore favor natural fractures that are oblique to the principal stress direction because these will be the ones with significant shear stresses acting on them. By increasing the hydraulic pressure acting on natural fractures that are already close to sliding, they can be mobilized. The stimulation of permeability in these cases is due again to breaking any cementing material that exists in the natural fractures and by dilation that naturally accompanies sliding of one rough crack surface with respect to another. These shearing mode fractures can also be considered to accompany opening mode fractures as fluid flows from the opening mode fracture into the intersecting natural fractures causing them to mobilize in shear.

FRACTURING DATA

A fracturing experiment was carried out at the Northparkes Mines E48 mine during the early stages of mine development. The goal of the project was to obtain data on growth of hydraulic fractures in the orebody, consisting of naturally fractured quartz monzonite and volcanic sediments. The site was located at the end of tunnel ED4 at a depth of 580 m below the surface. A 96 mm diameter core hole was drilled from the face of the tunnel, along its planned path. Five hydraulic fractures were then placed along a section of this borehole at distances of 70 to 130 m from the hole collar. The tunnel was then advanced along the borehole, passing through the 5 fractures, which were mapped as they were exposed at the tunnel face and sides. Figure 1 contains an oblique view of the site showing the tunnel system present at the time the hydraulic fractures were placed.

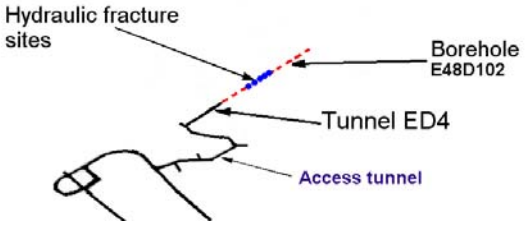

Figure 1: The fracturing was done in borehole E48D102 which was drilled from the face of tunnel ED4.

Site conditions

The rock mass making up the orebody at the site consists of hard volcanic sedimentary sequences intruded by quartz monzonite porphyry plugs. The rock is naturally fractured, containing many veins and approximately 6 fractures per meter. In addition, sub-vertical shear zones extend through the rock mass. Measuring the interaction of the hydraulic fractures with these large structures was an important goal of the experiment. A stereo plot showing the orientation of fractures mapped along the tunnel sides, after it was extended through the orebody, is shown in Figure 2.

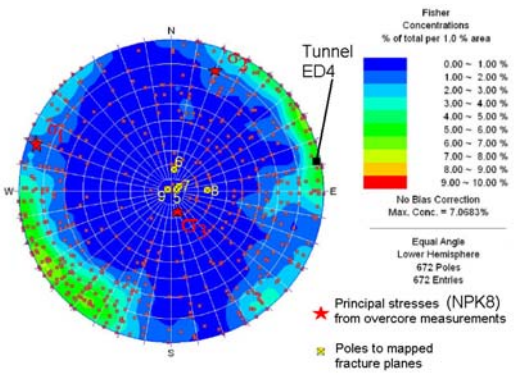

Figure 2: Stereo plot containing poles to natural fractures mapped along tunnel ED4. The principal stress vector directions and the tunnel direction are also shown.

The porphyry and volcaniclastic sediments are stiff rocks with core measured Young's modulus of 50 to 60 GPa and Poisson's ratio of 0.11 to 0.22. Their unconfined compressive strength ranges from 94 to 127 MPa. Figure 3 shows a photo of a core from the borehole (E48D102) section where the fracturing was carried out. The natural fracturing and veining can be seen in the core. Hydraulic fracture 9 was initiated at 69.7 m in this section of the borehole.

The in situ stress was measured after the tunnel was completed. Two measurements were made in one overcore hole. The stress measurement site was at 179 m from the collar of E48D102. The principal stresses were found to consist of a subvertical minimum stress and nearly horizontal maximum and intermediate principal stresses. Two overcore measurements were made within a 300 mm of one another. The principal stress magnitude reported here are averages from these two tests while the orientations are from test NPK8. The minimum stress was measured as dipping at 76 degrees with a magnitude of 15 MPa, consistent with the weight of the overburden at that depth. The intermediate stress was found to dip at 11 degrees and was oriented at 22 degrees with a magnitude of 22 MPa. The maximum principal stress was dipping at 8 degrees and oriented at 290 degrees with a magnitude of 40 MPa. Results from each test and additional detail about geology and rock properties are given in Jeffrey et al. (2009a).

Figure 3: Core from E48D102. The redish core is porphyry and the grey core is volcaniclastic.

Fracture treatments

Before the fracturing was started, a well test was carried out by pressurizing a 152 m long section of borehole E48D102 for 2.5 hours. This short test indicated the rock mass permeability was on the order of 0.005 milliDarcy.

Each hydraulic fracture treatment was carried out by isolating a 0.55m long section of the borehole using inflatable straddle packers. Table 1 provides a summary of the propped fractures placed.

Table 1: Summary of hydraulic fracture treatments in E48D102 at Northparkes

No	Straddle top (m)	Fluid	Volume (m^3)	Proppant
5	131.9	water	9.2	120 kg G
6	114.4	x-link	10.4	275 kg R
7	94.4	x-link	15.6	300 kg Y 500 kg 30/60 sand.
8	79.4	water	15.0	75 kg G 30 kg 30/60 sand
9	69.4	water	10.8	75 kg R

G – green, R – red, Y – yellow plastic

The colored plastic proppant ranged from 70 to 500 μm in size and was added to the fluid to clearly mark the fracture during mapping.

Figure 4 contains a summary plot of fracture treatment 5, which used water to place green plastic proppant. The average injection rate was nearly 400 Liters per minute during the time when plastic proppant was added.

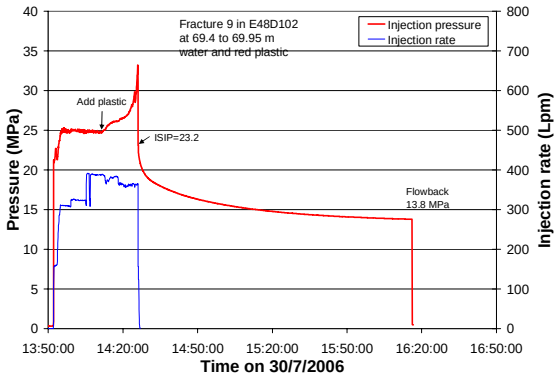

Figure 4: Summary plot of fracture treatment 9.

The plastic was large enough in particle size to have difficulty passing through the fracture channel, which caused the pressure to rise and eventually the treatment screened out. The crosslinked gel treatments did not suffer from screenout problems and more plastic and 30/60 mesh sand (250 to 600 μm in size) were placed in these gel treatments. The water based treatments had fluid efficiencies of approximately 50 percent, where the efficiency is the ratio of the volume of fluid contained in the fracture to the total volume injected. Therefore, half the fluid injected was lost into the surrounding rock during the injection period. This lost fluid induces an increase in pore pressure in the rock surrounding the hydraulic fracture. The gel treatments, as expected, suffered less fluid loss with efficiencies of approximately 90 percent. More details of the fracture closure and fluid efficiency calculations can be found in Jeffrey et al. (2009a). .

Mapped geometry

Immediately after the work of placing the fractures was complete, the mining of tunnel ED4 resumed. The tunnel was advanced in a mining cycle that involved drilling the face, loading and firing the holes in the face, clearing the broken rock, and supporting the newly exposed rock. Each cycle advanced the tunnel approximately 4 m and required 24 hours to complete. Most of the mapping of the hydraulic fractures was carried out during this mining cycle.

The fracture interaction and overall geometry data was collected by mine surveyors, digital photogrammetry, and digital photography. The mine survey and photogrammetry data were combined to provide coordinates of points along each fracture, giving the overall geometry and orientation. A DSLR camera, with tripod and flash unit, was used to capture photographs of the fracture as exposed in the tunnel face and walls. Figure 5 shows fracture 9 cutting across the face of the tunnel.

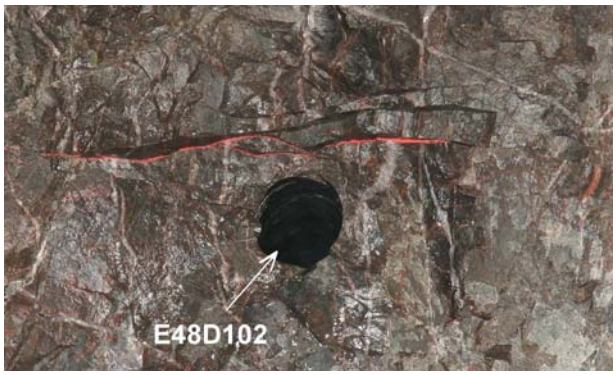

Figure 5: Fracture 9 is shown propped with red plastic running above hole E48D102 in the face of tunnel ED4 (after Jeffrey et al., 2009a).

Fracture 9 was following a pre-existing natural fracture at the location shown in Figure 5 although some fracture extension through fresh rock was present at the left and right tunnel walls. In addition, the segment of the fracture just above the borehole appears to be a location where two fracture fronts may have grown together. The lower branch of this part of the fracture was possibly extended as a new fracture through the rock. This interpretation is based on the curvature of the fracture just above the hole that follows the hole curvature, suggesting the fracture growth was affected by the reduced radial stress around the hole. Moving from right to left along this fracture, the curvature changes its nature and this portion of the fracture curves to grow into the fracture plane above it, as would be expected for the interaction of a fracture front with a second parallel fracture (Pollard et al., 1982). The fracture initiation point is located approximately 2 m ahead of this position, in the out of the paper direction. The fracture extended across the full tunnel width (nominally 5 m) but was not found after the next round was fired.

Figure 6 contains a composite drawing of all 5 mapped fractures with elevation, oblique and plan views show. The fractures are colored according to the color of the plastic proppant placed into each one. All of the fractures contained a number of offsets in their fracture path that developed, at some intersections with natural fractures, shear zones and veins. Six larger offsets have been numbered in Figure 6.and offset 1 is shown in the photo in Figure 8.

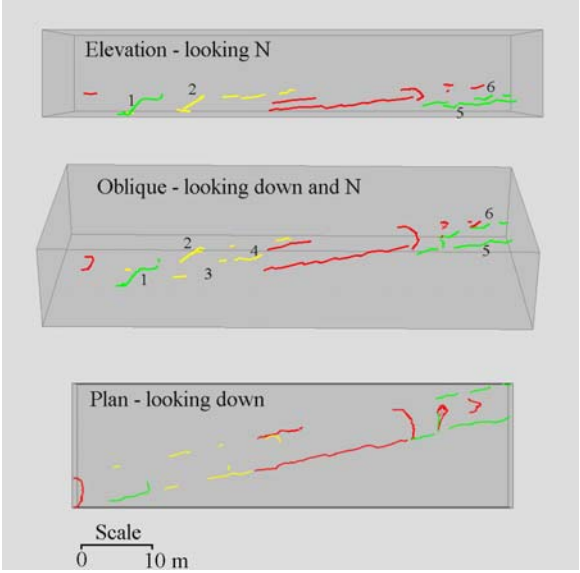

Figure 6: Three views showing the traces of the mapped fractures along tunnel ED4.

Mapping and analysis of fracture 8

Fracture 8 will be described in detail in this section because its geometry included large and small offsets, *en echelon* fractures and sub-parallel branches. The overall vertical section of fracture 8 along the south side of tunnel ED4 is shown in Figure 7.

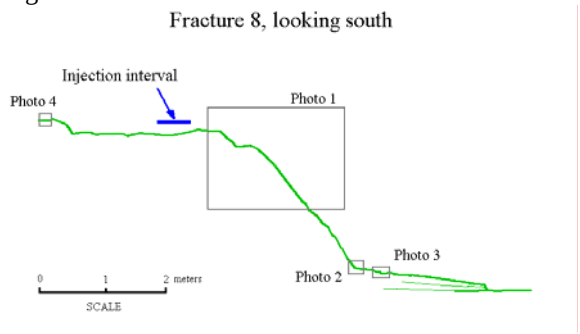

Figure 7: An elevation view of fracture 8 along the south wall of tunnel ED4. The injection interval is 2.5-3 m north of the fracture trace.

In Figure 8 (photo 1 in Figure 7), fracture 8 enters the large offset at the upper left. This structure dips at 45 degrees and contained quartz, sericite and calcite filling. Green plastic proppant was placed along this inclined structure, which indicates it was opened to a width of more than 1.5 mm during the injection.

Figure 8: Offset 1 (see Figure 7) in fracture 8, on the south side of ED4. The scale is 100 mm for each black and white segment.

A closer view of part of this offset portion of fracture 8 is shown in Figure 9. This figure shows the location indicated as photo 2 in Figure 7 where the fracture leaves the inclined structure. Figure 10 contains a photo taken just to the west of Figure 9 (labeled photo 3 in Figure 7).

Figure 9: A close view of fracture 8, on the south side of ED4, at the lower and west end of the inclined structure as it leaves the structure to become nearly horizontal again.

At this location, fracture 8 consists of overlapping segments with smaller offsets between them. Fracture 8 would have connected between these rock bridges either deeper in the rock or in the rock that was removed by mining.

Finally, a 20 mm offset is shown in Figure 11 which is located at photo 4 in Figure 7. The offset developed as the hydraulic fracture crossed a nearly vertical quartz-calcite vein.

Figure 10: Fracture 8 on the south side of ED4, a few meters to the west of the structure shown in Figure xx7. A sequence of en echelon fractures formed at this location.

Figure 12 contains a summary plot of the hydraulic fracture treatment for fracture 8. This treatment used water to form the fracture and the proppant included 75 kg of green plastic and 30 kg of 30/60 mesh sand. The treating pressure was nearly 10 MPa above the minimum stress magnitude before the proppant was added to the fluid. The pressure increased when proppant was added. Both high treating pressure and increasing pressure with the addition of proppant are considered diagnostic of complex fracture path development. In this case, the

Figure 11: Fracture 8 on the south side of ED4. A small offset is shown in the path of the fracture as it crosses a vein.

treatment was initiated near the large inclined structure and other offsets were present on both sides of the initiation interval. Note the injection interval is indicated in Figure 7 and was physically located in the center of the tunnel, 2.5 to 3 m to the north of this section along the tunnel wall. The dip of the

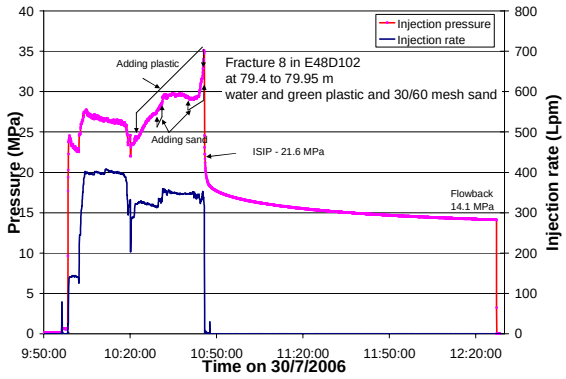

Figure 12: Treatment summary plot of fracture 8.

structure was 45 degrees with a dip direction of 245 degrees. A coordinate transformation can be applied to the measured principal stresses to estimate the normal and shear stress acting on this surface. When this is done, the normal and shear stress acting on the plane, arising from the far-field stress, are found to be σ_n = 26.3 MPa and τ = 10.3 MPa, respectively. The pressure early during fracture 8, before proppant was pumped, was 2 MPa or more higher than the pressure during fracture 9 and this higher pressure is consistent with a higher pressure needed to open the 45 degree dipping structure.

The Mohr circle diagram of the in situ stress state is contained in Figure 13. The normal and shear stress acting on the structure have been plotted in this diagram and a failure envelope has been drawn for a case where the pore pressure, induced by hydraulic fracturing, is either 15 or 22 MPa. For ease of plotting we have drawn the failure envelops displaced by the pore pressure value rather than the more usual practice of moving the stress circles to the left to account for the change in effective stress caused by the pore pressure increase. Under either pore pressure, slip is predicted to occur

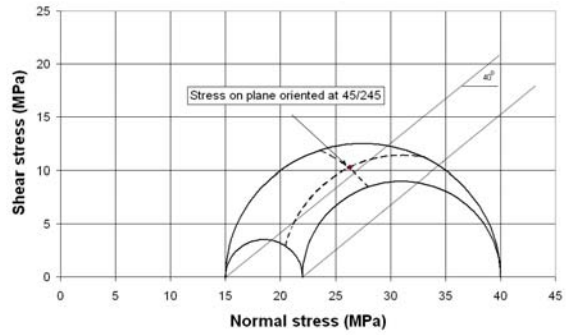

Figure 13: The measured stress state with the stress acting on the inclined structure intersected by fracture 8 indicated.

on the plane. The two orthogonal components of the shear stress vector are directed in the down dip direction (magnitude 7.7 MPa) and along the strike direction to the south (magnitude 6.8 MPa). These stresses impose mode II and mode III shearing on the fracture leading edge with some of this shear deformation transferred to the horizontal extension of the hydraulic fracture after it exits the inclined structure. The offset fractures seen in Figure 10 might then represent branching and *en echelon* fracturing induced by this shear deformation (Pollard et al., 1982). Alternatively, these *en echelon* fractures may have been pre-existing with the hydraulic fracture opening and following them. In both cases, the fracture path for fracture 8 and the *en echelon* fractures in Figure 10 are consistent with the direction of shearing imposed on this surface by the measured in situ stress field.

In general, fracture 8 and other hydraulic fractures at this site that were mapped consisted of main segments with a nearly horizontal orientation which were offset at fairly frequent intervals along inclined structures, most often stepping down when moving from east to west along the fracture. A typical mapped fracture contains many such offsets varying in size from a few millimeters to a meter or two in size.

To further investigate the effect of fracture growth through offsets, a number of numerical calculations have been made using a 2D displacement discontinuity based hydraulic fracturing model.

Numerical fracture modeling

The numerical model used here is based on the displacement discontinuity boundary element method. The model is capable of solving 2D plane strain hydraulic fracture problems involving viscous flow of Newtonian fluids. Fracture surfaces that are closed satisfy contact conditions and natural fractures are modeled as frictional discontinuities in an impermeable elastic rock mass. Details of the numerical formulation are contained in Zhang et al., (2005).

The model was applied to the problem of a hydraulic fracture with offsets along its path as shown in Figure 14. This geometry approximates the mapped geometry of fracture 8 in the plane of the tunnel wall. The rock properties and applied stresses are listed in the figure. The far-field stresses used in the model are the in-plane stresses arising from the 3D far-field stress. The goal is to reproduce qualitatively the pressure, opening and shearing response for fracture 8, but accepting the limitation imposed by the 2D approach and the fact that not every deflection of the fracture path is included in the geometry modeled. Nevertheless, the modeling serves to highlight important mechanisms that change hydraulic fracture pressure, width and growth rate when growing in naturally fractured rock masses. The numbers along

the fracture geometry sketch in Figure 14 refer to the offsets at those sites. These offsets are defined by their orientation angle (with respect to the x-axis direction) and their length. Table 2 lists the orientation and length of each of these offsets. A coefficient of friction of 0.8 is used for all surfaces that are in contact.

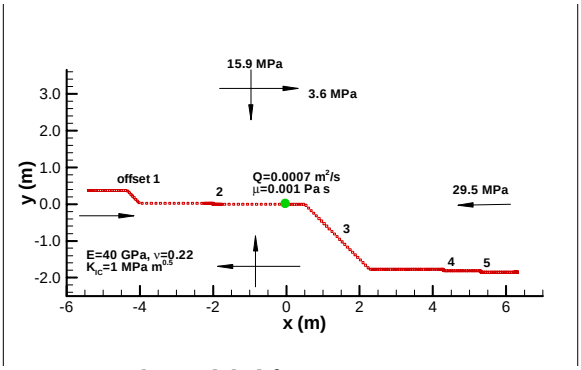

Figure 14: The modeled fracture geometry.

Table 2: Geometry of offsets for numerical model

Offset Number	1	2	3	4	5
Angle (deg)	135	90	-45	-60	-60
Length (m)	0.5	0.02	2.5	0.05	0.05

The fracture growth along the defined path was simulated by specifying the fluid injection rate and viscosity, with injection beginning at time t=0. Figures 15, 16, and 17 give the pressure, opening, and shear distribution along the fracture for 5 times during the simulation. The fluid penetrates further along the fracture as time increases, pressurizing more and more of it. Each offset acts to slow the advance of the fluid front because the offsets are acted on by higher normal stresses and have a higher opening stiffness (depending on their lengths).

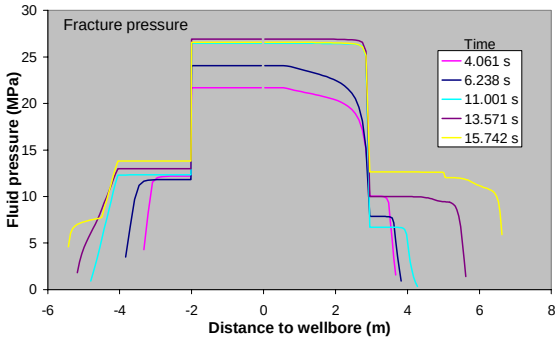

Figure 15: The pressure distributions in the fracture, at five times during injection, are shown.

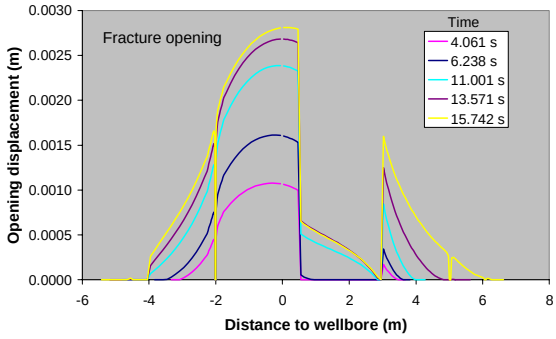

Figure 16: The opening displacement distributions in the fracture, at five times during injection, are shown.

An initial hydraulic width is specified for the fracture path and it is the conductivity associated with this initial width that allows the first fluid to enter and pass through each offset without the need to physically open the offset. The rate of growth of the fracture front and the pressure upstream of the offset, before it opens, are sensitive to the hydraulic width assigned to the fracture path. The results shown here were obtained using a hydraulic width of 0.01 mm everywhere except for offsets 3, 4 and 5, along which the hydraulic width was set to 0.05 mm. Along each segment, a parabolic shape is used for this hydraulic width distribution. It should be noticed that at the right end of offset 3, the hydraulic width is assigned 0.01 mm in this computation. The pressure distributions in Figure 15 show the high but nearly uniform pressure that develops in the central part of the fracture between offsets 2 and the right end of offset 3. Offset 3 restricts the fluid flow along it for the first two times shown but then is opened more widely except at its right end where a restriction persists. Offsets 2 and 3 remain the main restrictions to fluid flow. Large pressure gradients develop at the right end of offset 3 and at offset 2 as the fluid is forced through.

The opening displacements are consistent with the pressure distributions and clearly show the width restrictions that exist at the offsets. The pressure in the entire fracture acts to open it and this feature of an elastic fracture results in considerable opening width developing past the offsets, even without the pressure there exceeding the local normal stress acting on the fracture path.

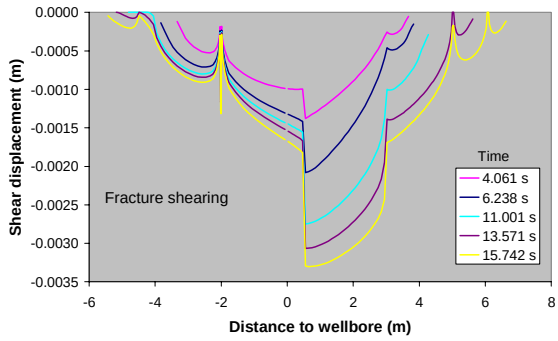

Figure 17: The shear displacement distributions in the fracture, at five times during injection, are shown.

The shear displacements calculated along the fracture at five different times are shown in Figure 17, illustrating how the far-field shear stress and the self-induced shear stress (Jeffrey et al., 2009b) acts to cause shear sliding on both the horizontal and inclined portions of the fracture path. As the pressure is reduced, after injection stops, some of the shear displacement will be locked in by the strength of the frictional surfaces. Figure 18 illustrates this behavior, which is a form of self-propping.

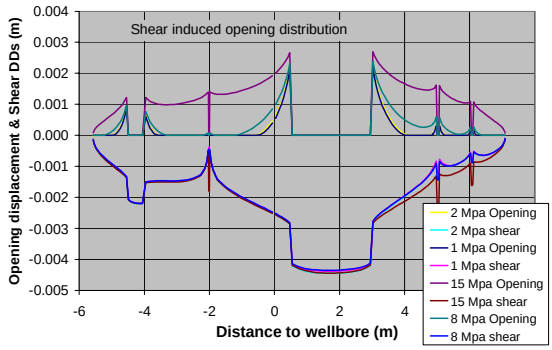

Figure 18: Fracture residual opening remaining as pressure is reduced.

The locked in shear displacement means that portions of the horizontal fracture cannot completely close. Hence, a significant portion of the fracture can be held open after the fluid pressure dissipates. The shear-induced opening at both ends of offset 3 is over 2 mm suggesting self propping in fractures with offsets can produce significant permeability enhancement even without placement of artificial proppant or considering the details of small-scale asperities.

Most of this permeability enhancement is generated by the shear slip occurring before opening, as illustrated by the opening curve in Figure 18 for a uniform pressure of 15 MPa. The problem with limiting the pressure to always be below the opening pressure is that it may require a very long time to pressurize a flow path sufficiently to allow large slip and associated self propping to occur. Injection at rates that produce opening mode hydraulic fracture growth requires higher pressures, but can extend fractures (and high pressures) to 100 m in less than an hour. Fluid lost from this high pressure channel into the surrounding rock mass will induce additional shear on natural fractures. In addition, proppant can be placed into the fracture near the wellbore if required to maintain a high conductivity path between the well and the main reservoir.

CONCLUSIONS

The mapped fracture geometry and numerical modeling of it show that opening mode hydraulic fractures can be effectively extended into naturally fractured rock. Furthermore, the fractures can be propped with sand or higher strength proppant even when injecting thin fluids, such as water, at moderate rates, provided the injection interval is short. Also, even in absence of sand proppant, the presence of offsets along the fracture path can be shown numerically to lead to a significant self-propping effect. Placement of a number of propped hydraulic fractures into an EGS reservoir along an injection or production well would provide improved access for injection of fluid to produce shear mode stimulation in the main reservoir and would reduce the near well flow impedance of the well during the main fluid circulation phase after stimulation. The mine through project reported on here has shown that:

1. The mapped hydraulic fractures in the naturally fractured rock mass were found to consist of primarily one propped channel. Branching to produce sections of multiple sub-parallel fractures did occur but made up only about 15 percent of the overall mapped extent.
2. The fractures consisted of horizontal sections that were offset at some intersection with natural fractures, shears, or veins. The fracture offsets typically produced a downward step in the fracture path when moving from east to west along the fracture path.
3. The stress field, hydraulic fracture orientation, and offset orientations mapped imply that considerable shear stress would be present on the path of the hydraulic fracture. Opening of the path will then produce shear displacement on the path, leading to some degree of self propping when the pressure is removed.
4. The spacing between the fractures was in general maintained over their mapped extent. Fracture 7 and 8 grew into the same plane at one location.
5. Proppant material, of up to 600 μm in size was placed into these fractures using water injected at 300 to 400 L/min. Using a more viscous gel fluid at the same injection rate

was more efficient in opening the fractures, with no screenout events recorded for the two crosslinked gel fractures.

6. Numerical modeling of an offset fracture geometry has demonstrated that higher injection pressures are required to extend the fracture through the stepped pathway but the portions of the fracture upstream of the next closed offset are opened more widely than they would be in a straight non-stepped fracture. This result may explain how the proppant could be placed using a low viscosity fluid such as water, injected at low rates.
7. The stepped fractures grew more slowly than straight fractures because of the greater fracture width upstream of the last offset.

ACKNOWLEDGEMENTS

The fracturing experiment at Northparkes was supported by a consortium consisting of Northparkes Mines, CSIRO, Shell E&P, Schlumberger, and Total E&P. We thank these companies for their support.

REFERENCES

Pearson, C.: (1981), The Relationship Between Microseismicity and High Pore Pressure During Hydraulic Stimulation Experiments in Low Permeability Granitic Rock, *Journal of Geophysical Research*, 86, No. B9, p 7855-7864, September 10.

Pine, R.J. and Batchelor, A.S.: (1984), Downward Migration of Shearing in Jointed Rock During Hydraulic Injections, *Int. Jour. Rock Mech. Min. Sci.* & Geomech. Abstr., 21, No. 5, p 249-263.

Pollard, D.D., Segall, P., and Delaney, P.T. (1982), Formation and interpretation of dilatant echelon cracks, Geol. Soc. of America Bulletin, 93, p1291-1303.

Jeffrey, R.G., Bunger, A.P., Lecampion, B., Zhang, X., Chen, Z.R., van As, A., Allison, D.P., de Beer, W., Dudley, J.W., Siebrits, E., Thiercelin, M. and Mainguy, M. (2009a), Measuring Hydraulic Fracture Growth in Naturally Fractured Rock, Paper SPE 124919 presented at the SPE Annual Technical Conference and Exhibition, New Orleans, Louisiana, 4–7 October.

Jeffrey, R.G., Zhang, X., and Thiercelin, M. (2009b), Hydraulic Fracture Offsetting in Naturally Fractured Reservoirs: Quantifying a Long-Recognized Process, Paper SPE 119351 presented at the SPE Hydraulic Fracturing Technology Conference, The Woodlands, Texas, 19-21 January.

Zhang, X., Jeffrey, R.G. and Detournay, E. (2005), Propagation of a fluid-driven fracture parallel to the free surface of an elastic half plane, *International Journal for Numerical and Analytical Methods in Geomechanics*, 29, pp. 1317–1340.

Zhang, X. and Jeffrey, R.G. (2008), Reinitiation or termination of fluid-driven fractures at frictional bedding interfaces. *J. of Geophysical Research*, 113 B08416, DOI:10.1029/2007JB005327.

Zimmermann, G. Reinicke, A., Brandt, W., Blocher, G., Milsch, H., Holl, H.-G., Moeck, I., Schulte, T., Saadat, A., and Huenges, E. (2008), Results of Stimulation Treatments at the Geothermal Research Wells in Gross Schoenebeck/Germany, Proceedings Thirty-Third Workshop on Geothermal Reservoir Engineering, Stanford University, Stanford, CA, Jan. 28-30.